BROWN DWARFS

Zones, spots, and planetary-scale waves beating in brown dwarf atmospheres

D. Apai,[1,2]* T. Karalidi,[1] M. S. Marley,[3] H. Yang,[1] D. Flateau,[1,4] S. Metchev,[5,6] N. B. Cowan,[7,8,9] E. Buenzli,[10] A. J. Burgasser,[11] J. Radigan,[12] E. Artigau,[9] P. Lowrance[13]

Brown dwarfs are massive analogs of extrasolar giant planets and may host types of atmospheric circulation not seen in the solar system. We analyzed a long-term Spitzer Space Telescope infrared monitoring campaign of brown dwarfs to constrain cloud cover variations over a total of 192 rotations. The infrared brightness evolution is dominated by beat patterns caused by planetary-scale wave pairs and by a small number of bright spots. The beating waves have similar amplitudes but slightly different apparent periods because of differing velocities or directions. The power spectrum of intermediate-temperature brown dwarfs resembles that of Neptune, indicating the presence of zonal temperature and wind speed variations. Our findings explain three previously puzzling behaviors seen in brown dwarf brightness variations.

Brown dwarfs are substellar and super-planetary in mass, but in size, temperature, composition, and chemistry, they are analogous to gas giant exoplanets (*1*). Isolated brown dwarfs are easier to study than exoplanets, making them valuable laboratories for investigating low-temperature (250 to 2000 K) atmosphere models. This includes the structure and dynamics of atmospheres, traced through observations of rotationally modulated variability and variations in spectral line profile shapes. Models of brown dwarf atmospheric dynamics predict two different types of circulation: a stable zonal pattern (rotationally dominated case) and stochastic, unstructured circulation (heat transport–dominated case) (*2*).

Heterogeneous condensate clouds (such as silicates) have recently been detected in brown dwarfs (*3*–*5*), offering tracers of the previously inaccessible atmospheric circulation of these objects. High-precision, time-resolved infrared observations sample the rotational phase dependence of disk-integrated emission, probing the distribution of clouds in a modest number of brown dwarfs (*5*, *6*). Rotational phase mapping studies have found that most if not all brown dwarfs have heterogeneous cloud cover (*7*, *8*); that the highest-amplitude rotational modulations in the 1- to 2.5-μm atmospheric windows are seen among objects at the transition between the silicate cloud-dominated L-type and the cooler (≲1300 K) T-types (*9*); and that the variability of L/T transition brown dwarfs is caused by simultaneous cloud thickness and brightness temperature variations (*3*–*6*, *10*). Brown dwarf light curves often display pressure-dependent phase shifts, revealing relatively complex longitudinal-vertical structures (*11*–*13*). Some brown dwarfs' light curves evolve in time (*3*, *12*, *14*, *15*), indicating vigorous atmospheric dynamics.

Despite this improving understanding, three types of prominent behavior remain confusing: (i) single-peaked (one peak per rotation) light curves splitting into double-peaked light curves (*4*, *12*); (ii) rapid transitions from very low-amplitude light curves (<0.5%) to high-amplitude ones (~5%) (*12*); and (iii) an apparently recurring feature in an otherwise irregularly evolving light curve (*15*). Atmospheric models based on elliptical spots (akin to the Great Red Spot on Jupiter) have been proposed to match or approximate light curve segments (typically a single rotation) (*3*, *5*, *15*), but no physically viable model has yet been proposed to explain the dramatic light curve evolution seen over a time scale of a few rotational periods.

We monitored a sample of ultracool brown dwarfs over 1.5 years, covering approximately 192 complete brown dwarf rotations (Fig. 1 and figs. S8 to S13). Our data sample atmospheric evolution over baselines up to 1000 rotations. The targets were brown dwarfs with known rotational modulations and with a range of temperature (800 to ~1500 K) and rotational periods (1.4 to 13 hours) (*16*). We observed each brown dwarf at eight epochs, each covering four complete rotations: Spitzer Channel 1 [central wavelength (λ_{cen}) = 3.6 μm; Ch1] observations of two rotations, followed by a single rotation in Channel 2 (λ_{cen} = 4.5 μm; Ch2), then one more rotation in Ch1. The data reduction was presented in (*12*) along with three initial results: (i) Rotational modulations were found in each visit; (ii) light curve evolution is seen in each target (over a single rotational period); and (iii) light curves that probe pressures <3 bar are coherent but offset in phase from the group of light curves that probe pressures >3 bar, indicating a vertical difference in cloud properties. For a given object, we found that similar rotational modulations are typically present in all three Ch1 rotations in a given visit, demonstrating that the lifetime of cloud features is longer than four rotational periods, corresponding to 52 hours in the case of the slowest rotating object (Fig. 1 and figs. S8 to S13). Continuous complex evolution is seen, and no two visits of the same target show identical light curves.

Here, we present new models that provide very good fits to all 24 light curves from our three high-amplitude L/T transition brown dwarfs (2MASS J13243553+6358281, 2MASS J01365662+0933473, and 2MASS J21392216+0220185; hereafter abbreviated as 2M1324, SIMP0136, and 2M2139, respectively). We first demonstrate our data and model fits on Visit 6 of 2M1324 (2M1324v6) (Fig. 1G), a particularly interesting segment with large amplitude evolution: The light curve evolves from a low-amplitude (<0.5%) state to a high-amplitude (>5%) one.

We introduce two models with different levels of realism: A simple analytical model and a numerical model based on atmospheric maps. Shown in Fig. 2 are examples for the two key atmospheric features we identified in the light curves and whose combination matches the observed light curve evolution: a longitudinal band with sinusoidal surface brightness modulations (Fig. 2A) and an elliptical bright spot (Fig. 2B). The band introduces a sinusoidal modulation in the disk-integrated light curve, and the elliptical bright spot introduces a positive (brighter) localized bump in the light curve.

Our analytical model sums three sine waves of different frequencies. It does not attempt to fit the few locations in our data that we identify as spots. In Fig. 1, the black lines show the best-fitting models. We investigated including a color term (f = Ch2 amplitude/Ch1 amplitude), but with the limited Ch2 data, this was not well constrained. The simple three-sine-wave model fits this complex light curve (Fig. 1G), with the exception of the periodically (four times) recurring features we attribute to a single bright spot rotating in and out of view (Fig. 1, "Spot"). The time difference between the first and last appearance of the spot indicates a rotational period of P_s = 13.2 hours at the (unknown) latitude of the spot.

Two of the sine waves derived in our model have very similar periods (P_1 = 14.32 hours and P_2 = 12.57 hours) and amplitudes (A_1 = 3.36% and A_3 = 3.39%). The slowly changing phase difference between these waves results in the beating effect known, for example, in acoustics: The combination of two higher-frequency constant-amplitude

[1]Steward Observatory, The University of Arizona, 933 N. Cherry Avenue, Tucson, AZ 85721, USA. [2]Lunar and Planetary Laboratory, University of Arizona, 1640 E. University Boulevard, Tucson, AZ 85721, USA. [3]NASA Ames Research Center, Moffett Field, CA 94035, USA. [4]Department of Physics, University of Cincinnati, 2600 Clifton Avenue, Cincinnati, OH 45221, USA. [5]Department of Physics and Astronomy and Centre for Planetary Science and Exploration, University of Western Ontario, London, ON N6A 3K7, Canada. [6]Department of Physics and Astronomy, Stony Brook University, Stony Brook, NY 11795-3800, USA. [7]Department of Earth and Planetary Sciences, McGill University, 3450 Rue University, Montreal, QC H3A 2A7, Canada. [8]McGill Space Institute, 3550 Rue University, Montréal, QC H3A 2A7, Canada. [9]Institut de Recherche sur les Exoplanètes (IREx), Département de Physique, Université de Montréal, C.P. 6128, Succ. Centre-Ville, Montréal, QC H3C 3J7, Canada. [10]Institute for Astronomy, ETH Zürich Wolfgang-Pauli-Straße 27, 8093 Zürich, Switzerland. [11]Center for Astrophysics and Space Science, University of California, San Diego, La Jolla, CA 92093, USA. [12]Department of Physics, Utah Valley University, 800 West University Parkway, Orem, UT 84058, USA. [13]Infrared Processing and Analysis Center, MS 314-5, California Institute of Technology, 1200 E. California Boulevard, Pasadena, CA 91125, USA.
*Corresponding author. Email: apai@arizona.edu

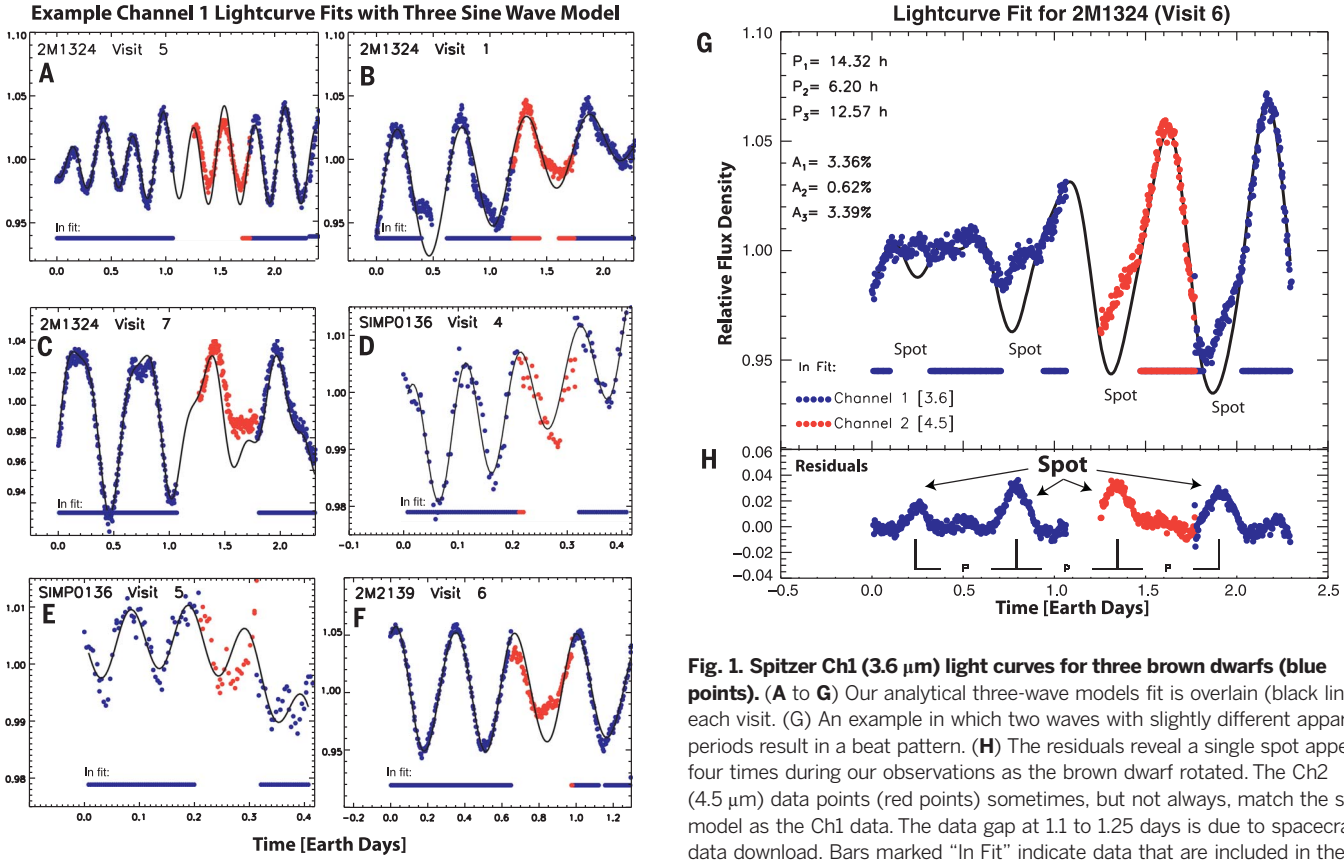

Fig. 1. Spitzer Ch1 (3.6 μm) light curves for three brown dwarfs (blue points). (**A** to **G**) Our analytical three-wave models fit is overlain (black line) for each visit. (G) An example in which two waves with slightly different apparent periods result in a beat pattern. (**H**) The residuals reveal a single spot appearing four times during our observations as the brown dwarf rotated. The Ch2 (4.5 μm) data points (red points) sometimes, but not always, match the same model as the Ch1 data. The data gap at 1.1 to 1.25 days is due to spacecraft data download. Bars marked "In Fit" indicate data that are included in the analytical fit, chosen to exclude regions affected by spots (gaps labeled as "Spot").

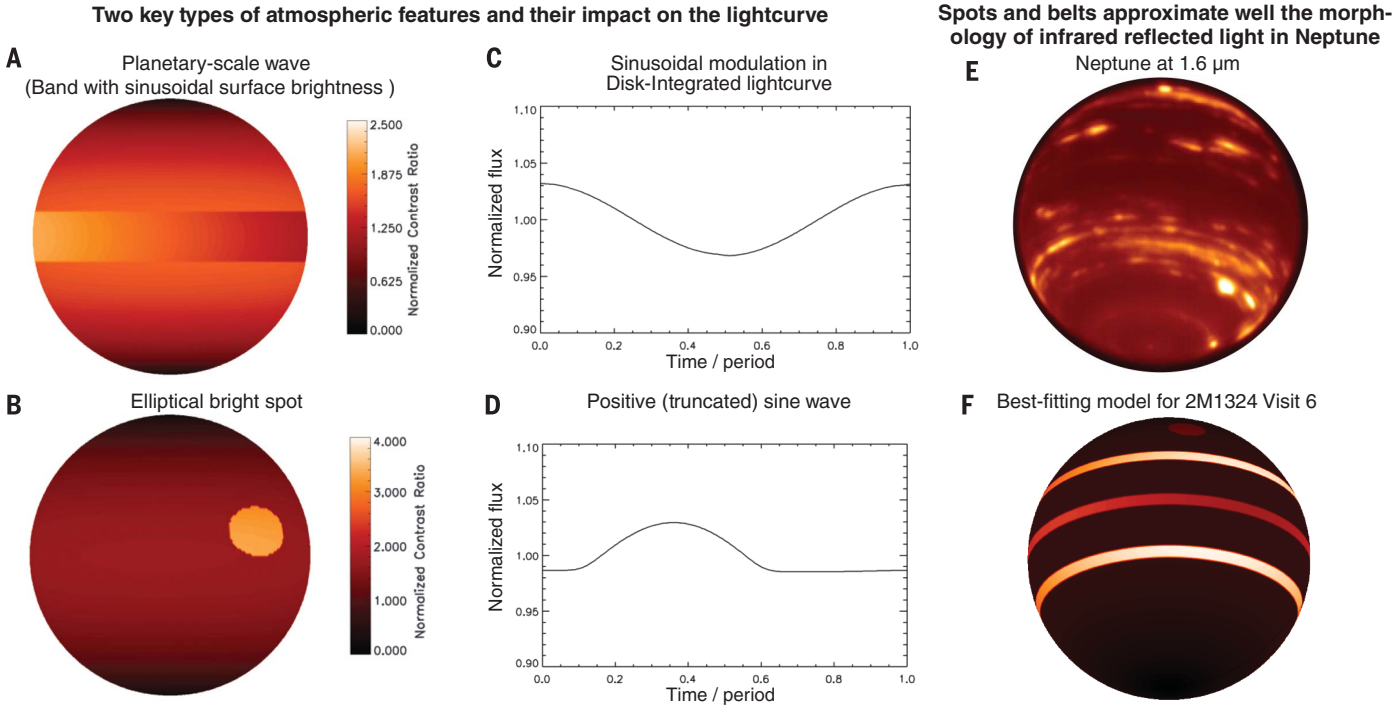

Fig. 2. The two key features (bands and spots) included in our light curve models and their appearance in the disk-integrated light curves. (**A** and **B**) Atmosphere models. (**C** and **D**) Disk-integrated light curves. Bands with zonal sinusoidally modulated surface brightness result in a sinusoidal temporal modulation in the light curve, whereas bright elliptical spots result in localized bright features. (**E**) The morphology of cloud features in Neptune observed in scattered near-infrared light (supplementary text). (**F**) Our best-fitting model of 2M1324 during visit 6.

waves produces a lower-frequency modulation in their sum. The mean of P_1 and P_3 is 13.44 hours, which is very close to the observed P_s = 13.2 hours rotational period of the spot. The third, higher-frequency wave's period is P_3 = 6.20 hours, half of the mean of P_1 and P_3 and also half of the spot's rotational period; we interpret this latter wave as a k = 2 wave, where k is the wavenumber.

We applied this analytical model to all eight visits of our targets. The model reproduces the light curves of the three L/T transition brown dwarfs (2M2139, 2M1324, and 2M0136), which are also the highest-amplitude objects in our survey. The data and model fits are shown in Fig. 1 and figs. S8 to S13). The probability distribution of the wave periods appearing in our analytical model for the three L/T dwarfs is shown in Fig. 3A. Given that the probability distributions of 2M1324 and 2M2139 are similar but have relatively low signal to noise ratios, we also show their combined probability distribution that may be representative to variable L/T dwarfs in general. As demonstrated in Fig. 3, the sine waves in the light curve evolution are most likely to appear at two or three distinct periods.

We have also applied Aeolus, an exoplanet-mapping software validated on Hubble Space Telescope Jupiter light curves and images (*17*), to multiple visits (Fig. 4 and figs. S1 to S3). The light curve is well reproduced, with three bands modulated with constant periods of P_1, P_2, and P_3 and with a bright spot. Disk-integrated observations necessarily result in information loss; therefore, our maps and interpretation cannot be considered unique. Instead, these models are the simplest maps that explain the data [for example, spot-only solutions with similar complexity could not fit the light curves over multiple rotations (supplementary text)].

Therefore, our two different approaches for modeling provide a consistent interpretation for the L/T brown dwarfs' light curve evolution: (i) The data for each brown dwarf can be modeled with two or three bands, each with sinusoidal brightness modulations; (ii) for the objects with three periods, two of the periods form wave pairs that bracket the reference rotation period of the object (the period of recurring spots); (iii) most visits also contain a single wave with half of the reference period; (iv) the slightly different periods of the wave pairs present in 2M1324 and 2M2139 result in lower-frequency amplitude modulation (beating); and (v) visits with high signal-to-noise (high-amplitude) light curves sometimes also show the presence of at least one additional, recurring bright spot.

Our results demonstrate that all three of our L/T brown dwarfs have planetary-scale modulations (wavenumbers k = 1 and k = 2) in their atmospheres; and at least two (2M2139 and 2M1324) have a wave pair in some visits. The brightness modulations seen may represent a single large wave but could also represent the envelopes of smaller features—bands composed of a large number of smaller features whose number density or brightness is modulated by the planetary-scale waves. Irrespective of any small-scale structure within these features, our data demonstrate that the disk-integrated modulations must be planetary-scale (k = 1 and k = 2).

The beating of planetary-scale wave pairs in L/T dwarfs also provides a single natural explanation for the three types of perplexing observations discussed above. First, the L/T transition dwarf Lu 16B exhibits recurring near-identical dark atmospheric features in light curves separated by hundreds of rotations (*15*). This finding can now be explained by a light curve driven by k = 1 waves (and not by elliptical spots). This results in light curves with characteristically shaped deep maxima and minima, when the phases of the two waves are matching. Second, the interplay of the two waves traveling at different speeds explains both the short-term and long-term light curve evolution seen in previous ground-based, lower signal-to-noise studies (*3*, *4*, *14*), in which the same brown dwarfs sometimes show single-peaked and sometimes double-peaked light curves. Double-peaked light curves are produced by our models when the phase shift between the two k = 1 waves is close to 90° (or 270°) or the k = 2 modes have greater amplitudes, whereas the light curves will appear single-peaked when the phase shifts are close to 0°. Third, variable brown dwarfs also occasionally appeared to be nonvariable; these episodic steady states appear in our model when the phase difference between the two nearly equal-amplitude waves is close to 180°. Examples of these behaviors in our data are shown in Fig. 1. 2M1324 displays these behaviors in our data; it is first a single-peaked light curve (Fig. 1C) but later becomes

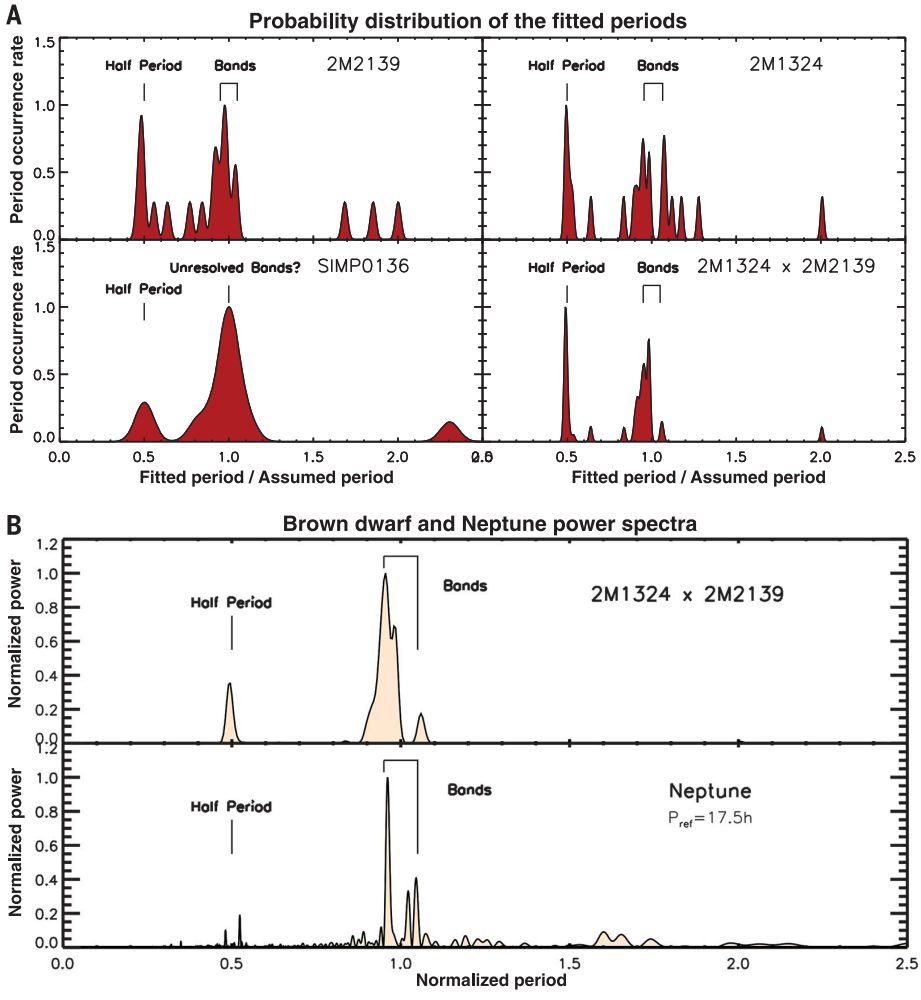

Fig. 3. Probability distributions and power spectra for the brown dwarfs and Neptune. (**A**) Probability distributions for the model periods of the sinusoidally modulated bands for the three L/T transition brown dwarfs and the combined probability for 2M1324 and 2M2139 (bottom right) from all our visits (single-visit fits). Data are from the analytical fits, and each period is represented as a Gaussian, with the estimated period uncertainty as its width. The distributions show wave pairs and a half period wave (k = 2 wave) in 2M2139 and 2M1324 and an apparently single band and a half period band in the short-period S0136. (**B**) Power spectra representative of the slower-rotating T2 dwarfs (2M1324 and 2M2139, shown as a product) and for Neptune [from (*18*)], extracted from Kepler optical photometry probing scattered light. The power spectra display similar peak distributions, once the lower time-resolution and sensitivity of the brown dwarf observations are taken into account.

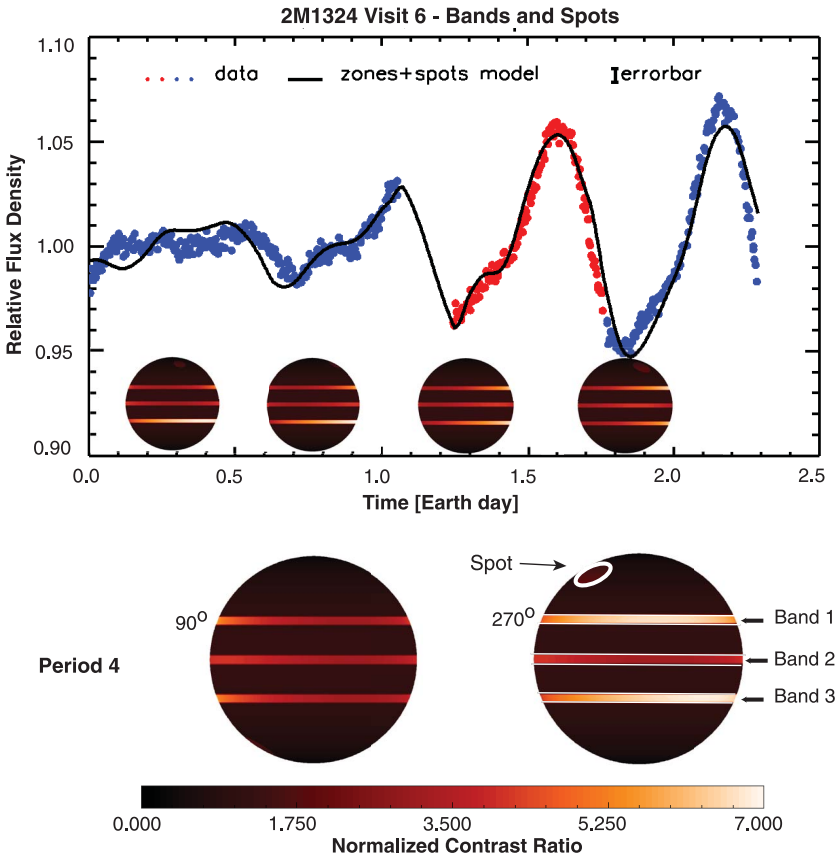

Fig. 4. MCMC model for 2M1324 visit 6. A Markov Chain Monte Carlo surface brightness model using Aeolus was fitted to the evolving light curve by using three sinusoidally modulated bands and a bright spot. The best-fitting model is very similar to our analytical model. The prominent light curve evolution is dominated by the beating effect caused by the phase shift between two modulations with slightly different periods. The four disks show the hemisphere facing the observer at the times corresponding to the center of each disk.

double-peaked (Fig. 1A), and at other times shows a period with very small amplitude (Fig. 1G, 0 to 0.9 days) followed by high-amplitude variations (Fig. 1G, 1.5 to 2.5 days).

Two of our targets' light curves are often dominated by wave pairs: for each pair, the amplitudes are very similar, and their periods are slightly but measurably different, symmetrically offset from the reference rotational periods of the target (Fig. 3). The differences between the wave periods and the nominal periods are $\Delta P_{1,2}$ = ±5% for 2M2139 (P_s ~ 8.2 hours) and $\Delta P_{1,2}$ = ±5.5% for 2M1324 (P_s ~ 13.2 hours). The symmetric differences between the shorter and longer periods and the spot-based rotational reference frame's period are naturally explained if the two bands are modulated by waves that are propagating prograde and retrograde with the same relative velocities (±Δv, eastward and westward winds, respectively). However, wave pairs propagating in the same direction but with velocities differing by 2Δv are also consistent with our data (both scenarios result in 2Δv wave propagation velocities). The latter scenario could be produced by differential rotation. Assuming a brown dwarf radius of 1.05 Jupiter radius (R_{Jup}) and waves close to the equator, the wave propagation speed is approximately $\Delta v = (\Delta P_1 + \Delta P_2)/2 \times 2R_{Jup}\pi/P_s^2$. We find Δv = 550 m/s for 2M1324 and Δv ~ 800 m/s for 2M2139, velocities similar to the maximum zonal wind speeds observed in Neptune (~300 to 400 m/s) and consistent with the wind speed upper limits suggested by spot-only models applied to single rotations (*3*–*5*, *13*). An intermediate Δv = 600 m/s velocity for the faster-rotating SIMP0136 (P_s = 2.43 hours) suggests that the apparent periods of the two k = 1 bands would differ by only 1%, which would be undetectable in our data. Therefore, although SIMP0136 shows a single k = 1 peak (Fig. 3) in our data, it may also have undetected multiple zones, similar to those in our slower-rotating targets.

In Fig. 3B, we compare the power spectrum of Neptune's optical scattered light photometric time series [from (*18*)] with the combined power spectrum of 2M1324 and 2M2139 (fig. S7). The combined power spectrum—the product of the probability distribution functions for the two similar objects—is used to illustrate the shared features and provides a representative higher signal-to-noise power spectrum. The combined power spectrum and that of Neptune show similar key features: the presence of multiple bands around the reference period and the presence of a half-period peak. For Neptune, the multiple peaks result from zonal winds: Neptune's circulation—very similarly to Uranus—is dominated by strong east-west jet streams confined to a shallow (~1000 km) atmospheric layer (*19*). Although the presence and stability of the zones in Neptune and Uranus are not fully understood, they coincide with alternating anomalously warm and cold temperatures, likely driven by adiabatic cooling and heating of rising and sinking plumes (*18*, *20*, *21*). Although Neptune's light curve is more complex than those of our targets and the brightness modulations are caused by clouds of various ices (CH_4, H_2S, NH_4SH, and H_2O) rather than silicate clouds, the similarity of the power spectrum and the rotational mapping results strongly suggest that our three brown dwarf targets also have a broadly Neptune-like zonal circulation with high zonal winds. Our interpretation of banded atmospheric circulation in brown dwarfs agrees with predictions of some circulation models (*2*, *22*) but demonstrates the unexpected importance of bands with varying brightness instead of large spots. We have also demonstrated a similarity between circulation in Neptune and brown dwarfs. Our results suggest that large-separation gas giant exoplanet candidates [such as HR 8799bcde (*23*) and HD 131399Ab (*24*)], which have near-identical temperatures to the brown dwarfs studies here, may also show banded circulation.

REFERENCES AND NOTES

1. A. Burrows, W. B. Hubbard, J. I. Lunine, J. Liebert, *Rev. Mod. Phys.* **73**, 719–765 (2001).
2. X. Zhang, A. S. Showman, *Astrophys. J.* **788**, L6 (2014).
3. É. Artigau, S. Bouchard, R. Doyon, D. Lafreniere, *Astrophys. J.* **701**, 1534–1539 (2009).
4. J. Radigan *et al.*, *Astrophys. J.* **750**, 105 (2012).
5. D. Apai *et al.*, *Astrophys. J.* **768**, 121 (2013).
6. E. Buenzli *et al.*, *Astrophys. J.* **798**, 127 (2015).
7. E. Buenzli, D. Apai, J. Radigan, I. N. Reid, D. Flateau, *Astrophys. J.* **782**, 77 (2014).
8. S. Metchev *et al.*, *Astrophys. J.* **799**, 154 (2015).
9. J. Radigan, D. Lafreniere, R. Jayawardhana, É. Artigau, *Astrophys. J.* **793**, 75 (2014).
10. A. Burgasser *et al.*, *Astrophys. J.* **785**, 48 (2014).
11. E. Buenzli *et al.*, *Astrophys. J.* **760**, L31 (2012).
12. H. Yang *et al.*, *Astrophys. J.* **826**, 8 (2016).
13. B. A. Biller *et al.*, *Astrophys. J.* **778**, L10 (2013).
14. M. Gillon *et al.*, *Astron. Astrophys.* **555**, L5 (2013).
15. T. Karalidi, D. Apai, M. S. Marley, E. Buenzli, *Astrophys. J.* **825**, 90 (2016).
16. Materials and methods are available online as supplementary materials.
17. T. Karalidi, D. Apai, G. Schneider, J. R. Hanson, J. M. Pasachoff, *Astrophys. J.* **814**, 65 (2015).
18. A. A. Simon *et al.*, *Astrophys. J.* **817**, 162 (2016).
19. Y. Kaspi, A. P. Showman, W. B. Hubbard, O. Aharonson, R. Helled, *Nature* **497**, 344–347 (2013).
20. I. de Pater *et al.*, *Icarus* **237**, 211–238 (2014).
21. J. Stauffer *et al.*, *Astron. J.* **152**, 142 (2016).
22. A. Showman, Y. Kaspi, *Astrophys. J.* **776**, 85 (2013).
23. C. Marois, B. Zuckerman, Q. M. Konopacky, B. Macintosh, T. Barman, *Nature* **468**, 1080–1083 (2010).
24. K. Wagner *et al.*, *Science* **353**, 673–678 (2016).

ACKNOWLEDGMENTS

Individual author contributions are listed in the supplementary materials. We acknowledge discussions with G. Mulders,

V. Parmentier, and X. Zhang on atmospheric dynamics and the interpretation of our observations. This work is part of the Spitzer Cycle-9 Exploration Program "Extrasolar Storms" and based in part on observations made with the Spitzer Space Telescope, which is operated by the Jet Propulsion Laboratory (JPL), California Institute of Technology, under a contract with NASA. Support for this work was provided by NASA through an award issued by JPL/California Institute of Technology. Support for the Hubble Space Telescope GO program 13176 was provided by Universities for Research in Astronomy, under NASA contract NAS5-26555. This research has benefitted from the SpeX Prism Spectral Libraries, maintained by A.J.B. at http://pono.ucsd.edu/~adam/browndwarfs/spexprism, and the M, L, T, and Y dwarf compendium at http://DwarfArchives.org. This research benefitted from the workshop "Solving the Exocartography Inverse Problem" held at the International Space Science Institute in Bern. The results reported here benefitted from collaborations and/or information exchange within NASA's Nexus for Exoplanet System Science (NExSS) research coordination network sponsored by NASA's Science Mission Directorate. An allocation of computer time from the University of Arizona Research Computing High Performance Computing and High Throughput Computing (HTC) is gratefully acknowledged. A.J.B. acknowledges funding support from the National Science Foundation under award AST-1517177. The raw observations are available from the Spitzer Heritage Archive at http://sha.ipac.caltech.edu under program 90063. Light curves for all of our targets, along with our model fits for each, are included in the supplementary file Data S1. Our adapted version of the Aeolus software is available at https://github.com/Dot83/Aeolus.

SUPPLEMENTARY MATERIAL

www.sciencemag.org/content/357/6352/683/suppl/DC1
Materials and Methods
Supplementary Text
Figs. S1 to S15
Tables S1 and S2
References (*25*–*34*)
Data S1

14 February 2017; accepted 25 July 2017
10.1126/science.aam9848

Science

Zones, spots, and planetary-scale waves beating in brown dwarf atmospheres

D. Apai, T. Karalidi, M. S. Marley, H. Yang, D. Flateau, S. Metchev, N. B. Cowan, E. Buenzli, A. J. Burgasser, J. Radigan, E. Artigau and P. Lowrance

Science **357** (6352), 683-687.
DOI: 10.1126/science.aam9848

Beating bands in substellar atmospheres

Brown dwarfs are objects with masses that are between those of large planets and small stars. They share many features with gas giant planets, particularly conditions in their atmospheres. Apai *et al.* analyzed how the infrared brightness of three brown dwarfs changes over time. Several perplexing features can be explained if bands of clouds rotating within their atmospheres generate beat patterns. Such bands are seen in optical images of Jupiter but best match infrared images of Neptune. The results shed light on the atmospheric physics of brown dwarfs and gas giant planets around the Sun and other stars.

Science, this issue p. 683